Delft University of Technology

Biomimetic design of a soft robotic fish for high speed locomotion

Van Den Berg, Sander C.; Scharff, Rob B.N.; Rusák, Zoltán; Wu, Jun

Citation (APA)
Van Den Berg, S. C., Scharff, R. B. N., Rusák, Z., & Wu, J. (2021). Biomimetic design of a soft robotic fish for high speed locomotion. In V. Vouloutsi, A. Mura, P. F. M. J. Verschure, F. Tauber, T. Speck, & T. J. Prescott (Eds.), *Biomimetic and Biohybrid Systems - 9th International Conference, Living Machines 2020, Proceedings* (pp. 366-377). (Lecture Notes in Computer Science (including subseries Lecture Notes in Artificial Intelligence and Lecture Notes in Bioinformatics); Vol. 12413 LNAI). Springer. https://doi.org/10.1007/978-3-030-64313-3_35

Important note
To cite this publication, please use the final published version (if applicable).
Please check the document version above.

Biomimetic Design of a Soft Robotic Fish for High Speed Locomotion

Sander C. van den Berg[0000−0001−7563−1622],
Rob B.N. Scharff[0000−0001−7996−4790], Zoltán Rusák[0000−0002−6999−5881], and
Jun Wu*[0000−0003−4237−1806]

Department of Sustainable Design Engineering, Delft University of Technology,
Landbergstraat 15, 2628 CE, Delft, The Netherlands
*Corresponding author: j.wu-1@tudelft.nl

Abstract. We present a novel DC motor driven soft robotic fish which is optimized for speed and efficiency based on experimental, numerical and theoretical investigation into oscillating propulsion. Our system achieves speeds up to 0.85 m/s, outperforming the previously reported fastest free swimming soft robotic fish by a significant margin of 27%. A simple and effective wire-driven active body and passive compliant body are used to mimic highly efficient thunniform swimming. The efficient DC motor to drive the system decreases internal losses compared to other soft robotic oscillating propulsion systems which are driven by one or multiple servo motors. The DC motor driven design allows for swimming at higher frequencies. The current design has been tested up to a tailbeat frequency of 5.5 Hz, and can potentially reach much higher frequencies.

Keywords: Soft robotic fish · Oscillating propulsion · Marine robotics · Biomimetics

1 Introduction

Minimal disruption to the marine environment is an important requirement for the design of underwater vehicles for closeup observations of marine life, (deep) sea exploration, mining, and pipeline inspection. Robotic fish using oscillating soft tails have advantages compared to underwater vehicles that use rotary propulsion. Rotary propulsion typically operates at a relatively high frequency. This creates highly disturbing vibrations in the water and actively sucks in objects and wildlife into the propeller. In contrast, oscillating propulsion uses lower frequencies and a compliant tail that pushes obstacles away rather than entangling them. Moreover, oscillating propulsion has the potential to be more efficient than rotary propulsion. This is due to the harvesting of energy from the turbulence at the wake of the vessel's body and the absence of energy losses due to rotation of the water flow as seen in rotary propulsion. Small propellers used to drive underwater vehicles typically do not produce efficiencies above 40% [13], where oscillating motion has shown efficiencies of up to 87% in lab experiments [2]. The difference in efficiency becomes especially large at great depths,
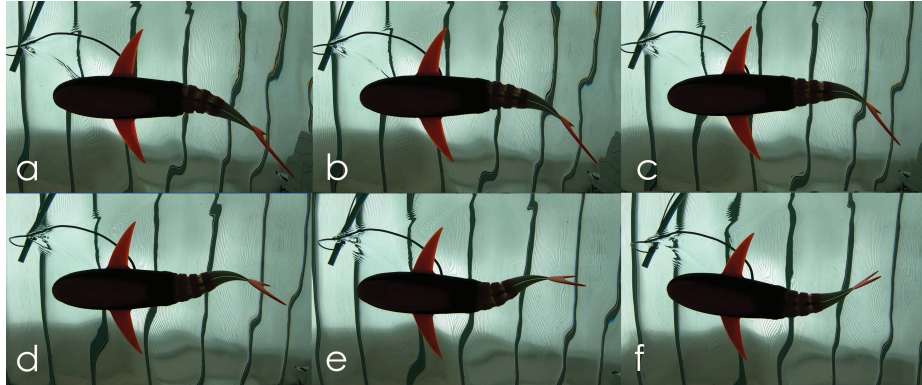
Fig. 1: Chronologically ordered snapshots of the soft robotic fish in action from a to f. A combination of an active and a passive tail segment is used to reproduce thunniform-like swimming.

where rotary propulsion systems have to exert large pressure on the rotary shaft to prevent water from seeping through, drastically reducing the efficiency of the system. In contrast, oscillating systems do not suffer from this problem as there are no rotating parts in contact with the water. However, the performance of the state-of-the-art soft robotic fish is still far from that of real fish and even from rotary propulsion in terms of both efficiency and speed. One of the reasons for this gap in performance is related to non-fluent motion of the tail of the robotic fish. In this work, we present a novel soft robotic fish design (see Fig. 1) by closely mimicking the fluent swimming motion seen in thunniform swimming.

Swimming speed of fishes depends on their propulsive mode. Accordingly, they are commonly classified according to their propulsive mode, which facilitates hydrodynamic analysis of swimming efficiency and performance. A commonly used classification by Lindsey [9] differentiates between twelve different swimming modes. Previous research has mostly focused on studying swimming modes that make use of the caudal fin and trunk to swim forward (i.e. anguilliform, subcarangiform, carangiform, and thunniform). Of these modes, thunniform swimming is known as the most efficient form of aquatic locomotion[11]. It uses the turbulence in the wake of the fish to create inwards turning vortexes on both sides. This produces a peak thrust in the middle behind the fish's tail, which is known as a reverse von Karman vortex street [3].

Different mechanisms for reproducing these fish-like oscillating motions have been proposed. A common approach is that of a multi-link system (see Fig. 2(a)). Here, the shape of the continuously curved tail is approximated by a series of rigid links that are controlled through internal or external motors. An example of a multi-link system is the RoboTuna [3]. An advantage of multi-link systems is the high degree of control on the oscillating motion due to the relatively high number of actuators. Therefore, multi-link systems are a popular choice for fish body kinematics studies [17].
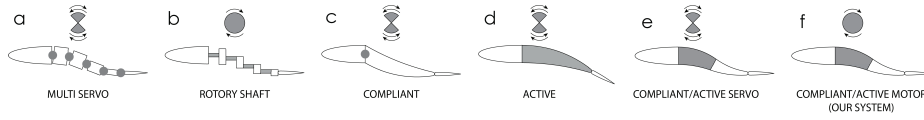
Fig. 2: Overview of robotic fish propulsion systems. The grey areas are actuated, whereas the white areas are passive. Grey dots are used to indicate actuated joints. The circle above each fish indicates whether the actuation is continuous or goes back-and-forth.

An effective propulsion mechanism is the use of a multi-link rotary shaft (see Fig. 2(b)). Generally speaking rotary shaft driven systems are able to reach a high speed due to their capability to produce very high frequencies. Here, a rotary shaft is led through hinging rigid links in the tail. Rotating the precisely curved shaft will create the oscillating motion. An advantage of this approach is that the motion of the robot stays the same for any tail beat frequency, allowing it to be tested at different frequencies without the need for modifications. However, its complex crankshaft design is prone to wear, and requires high precision fabrication. Moreover, the system does not allow for any easy steering mechanism. These limitations make it impractical to be used in practical applications. The Isplash fish makes use of this multi-link rotary shaft system [4]. A similar single rotary shaft mechanical solution with a single motor was presented by Yu et al. [18]. The recently reported Tunabot by Zhu et al. [20] also uses a single rotary shaft system resulting in record breaking speeds of 1.02 m/s at 15 Hz, although it should be mentioned that these results were not achieved in free swimming but by fixing the head in a laminar flow tank. Both multi-servo and rotary shaft systems lack compliance when interacting with underwater flora and fauna.

Taking inspiration from soft robotics, recent research focused on using an active compliant tail driven by fluidic actuators [6] (see Fig. 2(c)). Although the introduction of the soft tail makes the fish safer and more adaptive, the fluidic actuators were not capable of reproducing the sigmoid-like tail movement seen in thunniform swimming. As a result, the fish has a relatively low speed and efficiency.

In an attempt to simplify the control and design of these fishes, a fish with a passive compliant tail was proposed [1, 10] (see Fig. 2(d)). This solution has greatly reduced the complexity and costs of the system. However, this fish was not capable of accurately reproducing the sigmoid-like tail movement either. The free swimming fish presented in [10] reached a speed of 0.1 m/s, whereas the fish presented in [1] is slightly slower than that. This relatively low speed can be attributed to the sharp angle between the active and compliant part.

From there, an approach with a tail that contains both an active and a passive compliant part was proposed, enabling a smooth transition between the rigid head and compliant tail [19] (see Fig. 2(e)). This approach allowed for reproduction of reverse von karman vortices seen in thunniform swimming. Similarly to

the passive compliant body design, this design only requires a single servo motor, greatly reducing the complexity and increasing the efficiency as compared to the multi-link design. Using this system, a speed of 0.67 m/s could be obtained [19]. Although this system was a major step towards a viable system, the system still had some limitations. The servo-driven system creates an almost triangular waveform movement, whereas a more sinusoidal waveform would greatly improve the creation of reverse von Karman vortices [5]. Moreover, the maximum frequency of the servo-motor is limited. Therefore, the fish is unable to reach the tailbeat frequency needed to obtain a Strouhal number between 0.2 and 0.4, which is commonly found in nature and associated with energy efficient locomotion [12].

Our system (shown in Fig. 2(f)) solves the above mentioned challenges, resulting in a higher speed and efficiency. A key innovation of our system is the use of the continuous rotation of a DC motor to pull the cables connected to both sides of the active tail segment, instead of the commonly used back-and-forth motion of a servo-motor. As a result, higher frequencies can be obtained with a more sinusoidal waveform. Our fish is able to reach speeds up to 0.85 m/s. Hereby, it outperforms the previously reported fast soft robotic fish by Zhong et al. [19] with a significant margin of 27%. This significant performance improvement is an important step towards real-world applications of soft robotic fishes.

This paper is organized as follows: Section 2 presents the design of our soft robotic fish, emphasizing how the various components of the design can be optimized for speed and efficiency. Section 3 focuses the methods and materials used to fabricate and test our design. The results will be discussed in section 4. Finally, we conclude this work and discuss future work in Section 5.

2   Design

Our biomimetic design (Fig. 3) has a single-motor cable-driven oscillating system, in combination with a passive compliant tail segment to accurately reproduce thunniform swimming. The continuous rotation of the DC motor effectively pulls the cables connected to both sides of the active tail segment. The use of a DC motor allows for achieving higher frequencies with a more sinusoidal waveform, leading to improved speed and efficiency.

2.1   Motor

The soft robotic fish uses a DC-motor in combination with a gearbox system for propulsion, creating a motion as indicated in Fig. 2(f). Two gears on opposite sides of the motor shaft are rotated in opposite direction, pulling the left and right cable in a half cycle delay from each other, as illustrated in Fig. 4(a). As compared to the servo-motor driven system indicated in Fig. 4(b), a DC-motor driven active body allows for higher oscillation frequencies, and also creates a more cosine waveform of the active body and thus the caudal fin. In contrast, the
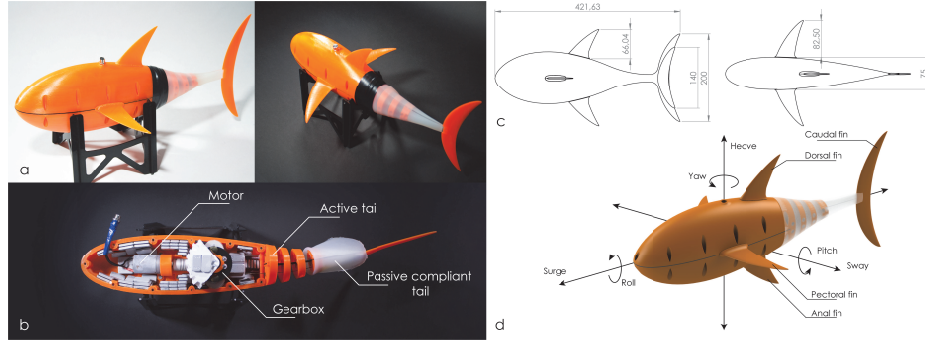
Fig. 3: (a) Design of the soft robotic fish, (b) internal view of the fish with the most important components indicated, (c) main dimensions of the soft robotic fish, and (d) terms for fish stability and fish anatomy.
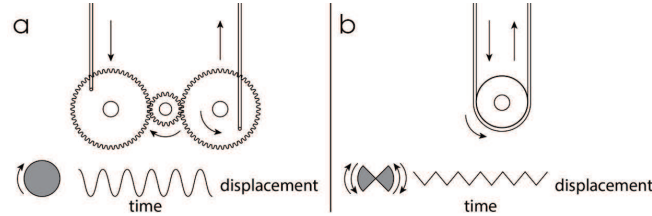

Fig. 4: On the left (a) the basic principle of our DC motor driven design. On the right (b), a servo-motor driven design. A graph of vertical displacement of the wires over time is depicted underneath both illustrations.

rapid change in direction in servo-motors leads to a triangle-like heave motion. Hover et al. have shown that sawtooth and square angle of attack profiles are approximately 20% less efficient than a sine profile [5].

2.2 Active and passive tail

The active part of the tail is composed of four rigid elements connected by three compliant joints. The stiffness of the passive tail segment should be chosen such that an S-shaped tail (as shown in Fig. 1(a)) is realized. An S-shaped tail creates a more optimal angle of attack of the caudal fin for creating thrust. Anderson et al. performed experiments with pitching and heaving foils in which the highest efficiency was obtained with a maximum angle of attack of 20.2 degrees with the direction of movement [2]. This is in line with previous research indicating an ideal maximum angle of attack of between $15°$ and $25°$ [13]. It should be noted that the stiffness that is required to obtain this ideal angle of attack is strongly dependent on the tailbeat frequency.

2.3   Body length

To investigate the influence of the body length on the maneuverability and sway stability, the behavior of a fish with an active and passive compliant tail segment was modeled as a mass-spring-damper system in *Simulink*. The simulation consists of four main segments: the caudal fin, the passive compliant segment, the active segment and the passive head, as is shown in Fig. 5. Both the compliant and active segments consist of multiple sub-segments to achieve sufficiently fluent motion. The passive compliant segment and active segment consist of 4 and 5 sub-segments respectively, with a length of 30 mm each. The rotation of the active segment is modeled to be constant over all sub-segments and varies over time following a sinusoidal function with a frequency of 1.59 Hz and amplitude of 5.73 degrees for each sub-segment.

The passive compliant segments were modeled having a consistent spring stiffness of 0.001 Nm/deg and a damping coefficient which was gradually reduced along the compliant segmentation from 0.005 Nm(deg/s) to 0.00075 Nm(deg/s) to simulate the decrease in surface area interacting with the surrounding water.

The body length was varied between 73.34 mm and 880 mm, corresponding to a ratio of head mass to total mass of 0.3 and 0.8 respectively. The distance between the centre of the caudal fin and the centre of rotation is used to express the maneuverability of the fish. The larger this distance is, the less maneuverable the fish is. The head sway stability is expressed as the angle between the passive head and the neutral line (indicated in blue in Fig. 5). A larger angle corresponds to a fish with lower sway stability. Lower sway stability leads to less efficient swimming, as energy is lost when the head is not aligned in the swimming direction. The results are shown in Fig. 6. A clear trade-off can be found between the maneuverability and sway stability. The tuna is an efficient long-distance swimmer with less need for quick maneuvers. Therefore, it has a relatively long body. We chose a similar length distribution for our robotic fish design (see Fig. 3(c)). At the same time, the relatively high length of the passive head provides space for the motor and gearbox.

2.4   Body shape & pectoral, anal, and dorsal fins

The body shape and the pectoral, anal, and dorsal fins of the fish greatly influence its stability and sway (see Fig. 3(d)). The vertically compressed elliptical body shape is inspired by the tunafish, and can be found in a large portion of fish species. Although the shape is not intuitive from a hydrodynamical point of view as minimizing drag around a given volume would result in a body of revolution, the advantage of this adaptation is the damping of the larger side surface area minimizing swaying motion during sideways oscillation of the tail [8]. Moreover, the shape also reduces rolling and creates a larger distance between the center of rotation and dorsal and anal fins, preventing change in vertical angle [15]. In fast swimming fish e.g. marlin, sailfish and mahimahi a large side surface area at a distance as far as possible from the center line of yaw rotation (defined by the line between the center of mass and buoyancy) is also a common adaptation.
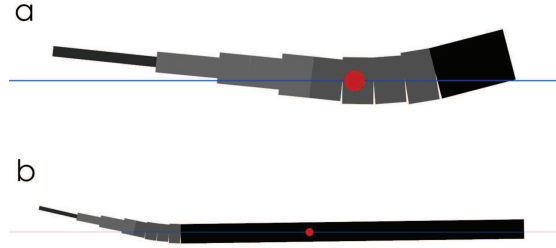
Fig. 5: *Simulink* model of the soft robotic fish. The different gray tones indicate the 4 main segments (from left to right: the tail, the passive compliant segment, the active segment and the passive head). The length of the passive head was varied between (a) 73.34 mm to (b) 880 mm. The centre of rotation is indicated in red. The neutral line is indicated in blue.

2.5 Caudal fin shape

The shape of caudal fin is critical for high-speed and efficient swimming. The caudal fin is illustrated in Fig. 3(d). When flapping the fin back and forth through the active and passive compliant tail, a pressure difference is generated between both sides of the caudal fin. The pressure difference generates vortices at the tip of the fin. The energy put in creating these vortices dissipates and produces drag. The vortices at high fins (and long wings in flight) are smaller compared to the total length over which the pressure difference is maintained, resulting in a higher efficiency [14]. The chord ratio (in aeronautics generally referred to as aspect ratio) is defined as the ratio between the caudal fin height (wing length) to the mean caudal fin width (mean chord length). The thrust-to-drag ratio (lift in aeronautics) increases with chord ratio, meaning that the higher the tail is relative to its width, the more efficient it swims [7, 2]. The caudal fin design has a backwards curving leading edge. Research has shown that a backwards curving leading edge was able to reduce drag by 8.8% as compared to a wing with the same chord ratio but a straight leading edge [16]. The caudal fins of highly efficient and fast long-distance swimming fish such as tuna closely match the design guidelines mentioned above. In contrast, fish that require high acceleration or maneuverability such as pikes have caudal fins with a much lower chord ratio. We perform experiments with a small caudal fin with a height of 140 mm and a larger caudal fin with a height of 200 mm (see Fig. 3(c)).

3 Fabrication & Experimental Setup

This section discusses the embodiment of the design and the setup that was used to evaluate its performance.
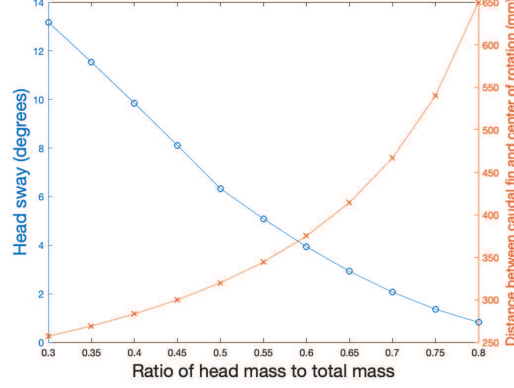
Fig. 6: Simulation results of the sway stability (circles) and maneuverability (crosses) versus the weight ratio of the head of the fish. The right axis indicates the distance between the caudal fin and the center of rotation, which is inversely related to the maneuverability.

3.1 Materials & fabrication

The body consists of four main components: the caudal fin, the passive tail, the active tail and the rigid body. The caudal fin is a lunate shape 3D-printed fin attached to the passive tail. The passive tail is a sheet which creates the desired bending at the desired tailbeat frequency and passive tail length. For this prototype, a 1 mm thick sheet of PETG of 74 mm length was used. The sheet follows the contour of the passive tail with a minimum height of 17 mm. The active tail is swept from side to side by two cables attached on both sides of the active tail. The active tail is supported by a compliant backbone sheet that functions as a compliant joint. The sheet has a thickness of 1.2 mm, length of 66 mm and height of 20 mm. Four rigid 3D-printed ribs are attached to the backbone to support the hydrodynamic shape and cables. The active and passive tail are encapsulated by a waterproof silicone skin, created from a 3D-printed mold. The rigid body consists of two 3D-printed halves held together by bolts and nuts with a rubber sealing ring in between. The bottom half holds a gearbox, sinkers, and the DC-motor (see Fig. 3(b)), while the top half holds a connector to an external power supply for precise power control during testing.

3.2 Measurement setup

A camera is placed parallel above the water. The camera (GoPro7) is set to linear settings to minimize deformation due to the lens, with a resolution of 1080 p, at 120 fps. As it is difficult to perfectly align the fish parallel to the water, calculations were performed to accurately determine the traveled distance speed. An example calculation is illustrated in fig. 7. The speed of the robotic

fish is measured by using the average length of a known segment of the fish to calculate the distance traveled divided by the time.
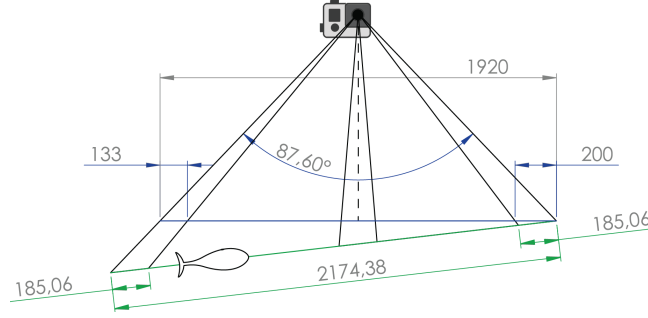

Fig. 7: The camera lens makes a horizontal angle of 87.6 degrees. In this example a segment of the fish with a known length 0.2481 m is 133px at the beginning of the measurement and 200 px at the end of the measurement. Taking into account the projection the known segment of 0.2481 m is 185.06 px and has traveled a total of 2174.38 px within the frame.

The speed is measured from the lowest voltage at which the motor starts turning, which is 5 V. The voltage is increased by increments of 0.5 V till failure of the prototype or the maximum specification of the motor are reached. At each voltage the experiment is repeated until at least three good straight swimming samples were captured. The tail sweep amplitude of the robotic fish is measured when the robotic fish is in the middle of the camera view in order to minimize any field of view deformation. The length of the tail sweep amplitude is compared to the reference length onscreen of which the real length is known. The efficiency of the fish is measured through the Strouhal number, which can be calculated as:

$$St = \frac{f * A}{U} \tag{1}$$

where f is the tail beat frequency, A is the tail sweep amplitude and U is the speed. The Strouhal number is a dimensionless number, which is found to be between 0.2 and 0.4 for energy-efficient locomotion [12].

4 Results

The swimming performance of the biomimetic soft robotic fish is presented in this section. The supplementary video (https://www.youtube.com/watch?v=tvL4VXgySOI) demonstrates that our biomimetic robotic fish is capable of reproducing a thunniform-like swimming motion through the combination of an active and passive tail segment. Fig. 8 shows the speed of the soft robotic fish for different tailbeat frequencies for the small caudal fin as well as the larger caudal fin. It can be seen

that higher speeds could be obtained when using the larger caudal fin. A top speed of 0.85 m/s (2.02 BL/s) was achieved at a tailbeat frequency of 5.46 Hz.
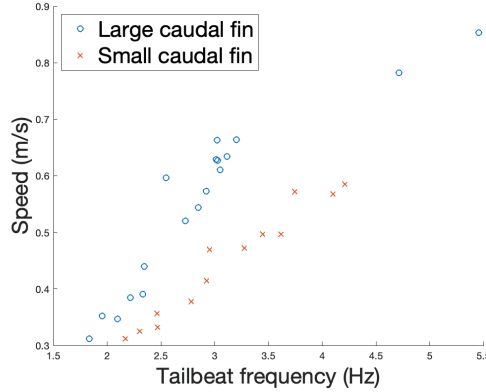

Fig. 8: Forward speed over tailbeat frequency for both the small as the large caudal fin.

Fig. 9(a) shows the tail sweep length versus the tailbeat frequency. Note that the tailbeat frequencies between the experiments with the small and large caudal fin do not match, as applying a certain voltage will result in different tailbeat frequencies for the two designs. It can be seen that up to a tailbeat frequency of 2.2 Hz, the tail sweep length of the fish with the large caudal fin increases with an increase in tailbeat frequency. This can be explained by the tail moving in its eigenfrequency, causing it to overbend. At higher frequencies, the tail sweep length starts to decrease due to deformation of the passive tail segment resulting in a more S-shaped tail (as shown in Fig. 1(a)). This is associated with higher efficiencies as the caudal fin has a more optimal angle of attack. This is confirmed by Fig. 9(b), where the Strouhal number approaches more optimal values (0.2-0.4) with an increase in tailbeat frequency. For the robotic fish with the large caudal fin, Strouhal numbers between 0.31 and 0.4 could be achieved at frequencies above 2.33 Hz. For reference, the servo-driven soft robotic fish by Zhong et al. [19] achieved Strouhal numbers between 0.36 and 0.6.

5   Conclusion

This work presented a biomimetic design of a soft robotic fish for high-speed locomotion. During free swimming, the fish achieved a top speed of 0.85 m/s, outperforming previously reported fastest free swimming soft robotic fish by a significant margin of 27%. At higher tailbeat frequencies, the speed of the fish increased, whereas the tailsweep length decreased due to a more sigmoid-like tail shape resulting in a more optimal angle of attack. At a tailbeat frequency
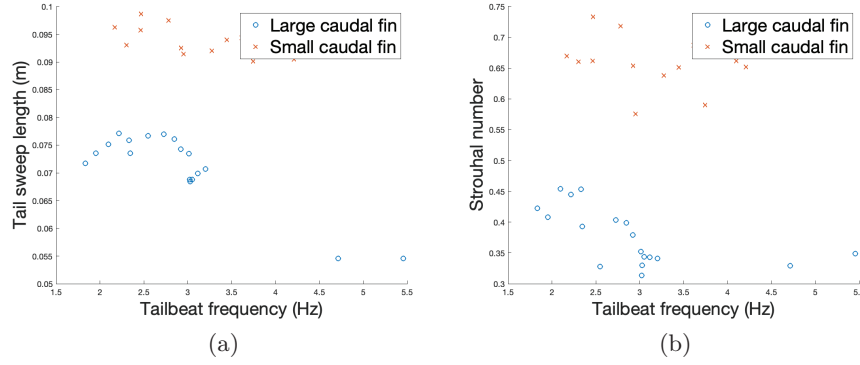
Fig. 9: (a) Tail sweep length over tailbeat frequency for both the small as the large caudal fin. (b) Strouhal number over tailbeat frequency for both the small as the large caudal fin.

above 2.33 Hz, the Strouhal number of the prototype with the large caudal fin dropped below 0.4, which is an indicator of good efficiency. These results confirm the theoretically predicted gain in efficiency due to the increased tailbeat frequency and more sinusoidal waveform enabled by our novel propulsion system design. The stiffness of the passive tail segment should be tuned to the tailbeat frequency such that a sigmoid-like tail shape and optimal angle of attack is achieved. Future work will focus on controlling the stiffness of the passive tail segment dynamically in order to achieve efficient swimming at different speeds. Although our propulsion mechanisms allows for a relatively easy implementation of a steering mechanism, it has not been implemented in this prototype. This will be part of future work as well. The design of the soft robotic fish will be made available online.

References

1. y Alvarado, P.V., Youcef-Toumi, K.: Modeling and design methodology of an efficient underwater propulsion system. In: Robotics and Applications. pp. 161–166 (2003)
2. Anderson, J., Streitlien, K., Barrett, D., Triantafyllou, M.: Oscillating foils of high propulsive efficiency. Journal of Fluid Mechanics **360**, 41–72 (1998)
3. Barrett, D., Triantafyllou, M., Yue, D., Grosenbaugh, M., Wolfgang, M.: Drag reduction in fish-like locomotion. Journal of Fluid Mechanics **392**, 183–212 (1999)
4. Clapham, R.J., Hu, H.: iSplash: Realizing fast carangiform swimming to outperform a real fish. In: Robot Fish, pp. 193–218. Springer (2015)
5. Hover, F., Haugsdal, Ø., Triantafyllou, M.: Effect of angle of attack profiles in flapping foil propulsion. Journal of Fluids and Structures **19**(1), 37–47 (2004)
6. Katzschmann, R.K., DelPreto, J., MacCurdy, R., Rus, D.: Exploration of underwater life with an acoustically controlled soft robotic fish. Science Robotics **3**(16), eaar3449 (2018)

7. Kermode, A.C.: Mechanics of Flight. Longman (1987)
8. Lighthill, M.J.: Aquatic animal propulsion of high hydromechanical efficiency. Journal of Fluid Mechanics **44**(2), 265–301 (1970)
9. Lindsey, C.: 1 - form, function, and locomotory habits in fish. In: Hoar, W., Randall, D. (eds.) Locomotion, Fish Physiology, vol. 7, pp. 1 – 100. Academic Press (1978)
10. Mazumdar, A., Alvarado, P.V.Y., Youcef-Toumi, K.: Maneuverability of a robotic tuna with compliant body. In: 2008 IEEE International Conference on Robotics and Automation. pp. 683–688. IEEE (2008)
11. Sfakiotakis, M., Lane, D.M., Davies, J.B.C.: Review of fish swimming modes for aquatic locomotion. IEEE Journal of oceanic engineering **24**(2), 237–252 (1999)
12. Triantafyllou, G.S., Triantafyllou, M., Grosenbaugh, M.: Optimal thrust development in oscillating foils with application to fish propulsion. Journal of Fluids and Structures **7**(2), 205–224 (1993)
13. Triantafyllou, M.S., Triantafyllou, G.S.: An efficient swimming machine. Scientific american **272**(3), 64–70 (1995)
14. Videler, J.J.: Fish swimming. Springer Science & Business Media (2012)
15. Weihs, D.: Stability versus maneuverability in aquatic locomotion. Integrative and Comparative Biology **42**(1), 127–134 (2002)
16. Westerhoff, H.V., Van Dam, K.: Thermodynamics and control of biological free-energy transduction. Elsevier Science Ltd (1987)
17. Wu, Z., Yu, J., Tan, M., Zhang, J.: Kinematic comparison of forward and backward swimming and maneuvering in a self-propelled sub-carangiform robotic fish. Journal of Bionic Engineering **11**(2), 199 – 212 (2014)
18. Yu, J., Zhang, C., Liu, L.: Design and control of a single-motor-actuated robotic fish capable of fast swimming and maneuverability. IEEE/ASME Transactions on Mechatronics **21**(3), 1711–1719 (June 2016). https://doi.org/10.1109/TMECH.2016.2517931
19. Zhong, Y., Li, Z., Du, R.: A novel robot fish with wire-driven active body and compliant tail. IEEE/ASME Transactions on Mechatronics **22**(4), 1633–1643 (2017)
20. Zhu, J., White, C., Wainwright, D.K., Di Santo, V., Lauder, G.V., Bart-Smith, H.: Tuna robotics: A high-frequency experimental platform exploring the performance space of swimming fishes. Science Robotics **4**(34) (2019). https://doi.org/10.1126/scirobotics.aax4615